

### RESEARCH PAPER

# Numerical analysis of the propagation modes of photo-switching PDMS-arylazopyrazole optical waveguide and thin-film spectroscopic characterization

Golsa Mirbagherio, a,\* Ikemefuna Uba, a Kesete Ghebreyessus, b Uwe Hömmerich,<sup>c</sup> Seth Fraden,<sup>d</sup> Michael Stehnach,<sup>d</sup> and Demetris Geddis<sup>a</sup>

<sup>a</sup>Hampton University, Department of Electrical and Computer Engineering, Hampton, Virginia, United States <sup>b</sup>Hampton University, Department of Chemistry and Biochemistry, Hampton, Virginia, United States <sup>c</sup>Hampton University, Department of Physics, Hampton, Virginia, United States <sup>d</sup>Brandeis University, Physics Department, Waltham, Massachusetts, United States

ABSTRACT. A new light-responsive arylazopyrazole (AAP) containing a polymer matrix thin film is fabricated by spin-coating different concentrations of the AAP azo dye into the polydimethylsiloxane (PDMS) polymer at 150°C. The new AAP molecular switch was also used to fabricate a solid-state PDMS-AAP waveguide by contact lithography and soft replica modeling methods in the micrometer scale. The refractive index of the spin-coated photoswitchable material can be modulated via the reversible trans-to-cis photoisomerization behavior of the AAP unit using different concentrations. When 0.01 M solution of the AAP unit was used, the refractive of the composite was 2.32 in the trans state and dropped to 1.85 in the cis state in the operating wavelength of 340 nm. At higher concentrations of 0.020 and 0.03 M, a wide refractive index tuning is achieved under the same wavelength. In 0.030 M, the refractive index was 2.65 for the trans state and 2.0 for the cis state. The results suggest that the increase in refractive index tuning is related to the concentration of the AAP unit of the composite film. Theoretically, the spectral properties of the composite film are also simulated with two methods: (1) the Maxwell equations and (2) the frequency dependent finite element, showing excellent agreement for the different propagation modes of the proposed waveguide for regulated signals of 365/525 nm wavelengths. Furthermore, the photoisomerization of the PDMS-AAP thin film is analyzed with UV-vis spectroscopy to demonstrate the isomerization responses of the AAP moiety in the solid state. In addition, preliminary photomechanical actuation properties of the composite film have been investigated. The PDMS-AAP waveguide described provides a new approach for optically tunable photonics applications in the UV-visible region.

© 2023 Society of Photo-Optical Instrumentation Engineers (SPIE) [DOI: 10.1117/1.JNP.17.026014]

**Keywords:** optical waveguide; photoswitchable materials; PDMS; arylazopyrazole; photoisomerization

Paper 23030G received Mar. 6, 2023; revised Jun. 13, 2023; accepted Jun. 13, 2023; published Jun. 24, 2023.

<sup>\*</sup>Address all correspondence to Golsa Mirbagheri, golsa.mirbagheri@hamptonu.edu

# 1 Introduction

Photoresponsive smart materials with properties that can be reversibly switched between two distinct states by light stimulus have been widely developed in diverse optochemical platforms. Previous work on photoresponsive materials that undergo light-induced reversible *trans-to-cis* conformational changes has mostly been concentrated on the highly versatile azobenzene photoswtiches. Azobenzenes undergo photo-induced *trans-to-cis* isomerization upon exposure to light of specific wavelengths. Despite their remarkable success, azobenzenes often suffer from two performance issues: incomplete switching or low thermal stability of the metastable *cis*-isomer. Arylazopyrazoles (AAPs) have been recently introduced as superior analogues of azobenzenes characterized by near quantitative conversion between two states and superior thermal half-life times of the metastable state. AAPs undergo efficient reversible *trans-to-cis* photoisomerization upon alternating irradiation with UV or green light to achieve a conformational change. The facile synthetic access and the superior optical properties of AAPs make them a favorable choice in the fabrication of guided optics, optoelectronics, and optofluidic platforms. A10

The change in molecular configuration leads to a significant change in electronic and steric structure, and thus allows for switching of intrinsic material properties. One of the intrinsic material properties addressed in this study is refractive index. The photochemical modulation of the refractive index in polymeric materials and their composites is of significant interest for optical applications, such as polymeric waveguides, optical switches, and optical data storage devices. Therefore, due to the important role of the refractive index in polymeric material, photochemically induced index modification in photonic devices gained considerable attention. Tuning the propagation modes of the waveguide modifies the strength of the interaction force between the waveguide channels. <sup>10,12</sup> One way to inspect this tuning is through the embedding of photochromic organic molecules into the polymeric waveguides. However, while there are many examples of photoresponsive waveguides formed by an azobenzene based polymers that can achieve refractive index modulation upon illumination with specific wavelength of light, <sup>1,2</sup> to the best of our knowledge, there are only few reported studies of polymeric waveguides based on the novel AAP molecular switches. <sup>10,11</sup> Hence, this study aims to exploit the novel properties of the AAP molecular switches for the development of new photoswitchable light responsive polymeric waveguides that would enable the reversible photomodulation of the refractive index of azo polymer composite films.

We have previously demonstrated the fabrication of PDMS-AAP composite thin films and studied the refractive index changes through the trans-to-cis isomerization of the AAP unit embedded in the polymer matrix.<sup>6,9,10</sup> The PDMS-AAP matrix exhibits 100% light-triggered reversible efficiency, with maxima refractive index change during isomerization process. 10,13,14 In this work, we have extended the study through the design of new AAP based molecular switch and its use for the fabrication of PDMS-AAP based waveguide, where the index of PDMS-AAP composite core is adjusted in-situ by alternating exposure to UV and green light. The immersed core simulated in Sec. 2 is surrounded by flexible PDMS clad which is transparent in the UVvisible region. Our previous study demonstrated the feasibility by closed-form analysis of Maxwell equations and illustrated the electric field modes of the guided light in the PDMS-AAP core.<sup>10</sup> In Sec. 2, the fabrication of the PDMS-AAP composite film is carried out by spin-coating of the different concentrations of the AAP and PDMS units and baked at 150° C. Then, we outline the fabrication of the PDMS replica mold with soft lithography. The contact photolithography method described in this study is used to make the PDMS grooves in a micrometer scale. This initial study is undertaken with the goal of expanding the soft lithography technique for the fabrication of nanoimprint lithography to create nano-grooves of the PDMS. <sup>15,16</sup> In Sec. 3, the simulation of the waveguide is performed by illustrating the electric field modes of the guided light into the PDMS-AAP core through numerical finite element method. 17,18 The photoisomerization behavior of the photochromic molecules embedded in the composite thin film characterized by UV-vis spectroscopy through alternating exposure of the core to 365 and 525 nm wavelengths as described in Sec. 4. In addition, the mechanical properties of the composite thin film are investigated by regulating the UV and green lights, resulting in a slight nanoscale bending actuation due to isomerization of the AAP molecules embedded in the polymer matrix. Material tunability is essential for the unlocking of potential practical applications of photoswitchable nanophotonic devices and systems. <sup>19–21</sup> The work presented here demonstrates clearly reversible light-responsive tuning of refractive index of polymer composite films with potential applications in diverse fields, such as stress sensing optoelectronics applications, sensors and soft robotics. <sup>22</sup>

# 2 Experimental Section

#### A. Material

All reagents were commercial grade and used as received without further purification.

#### B. Preparation of the composite

Commercial Sylgard 184 PDMS kit from Dow Corning Inc. was mixed in the standard 10:1 ratio using  $1.0\pm0.04$  g elastomer and  $0.1\pm0.02$  g curing agent. Appropriate amounts of the AAP were dissolved in acetone to make 0.01M, 0.02M, and 0.03M solutions. 50  $\mu$ L of each molar solution were added to dedicated PDMS mixtures, stirred manually with glass rod, and then deposited on previously cleaned glass substrates via spin-coating at 1000 rpm. The high spin speed eliminated the need to degas the blend prior to coating. The coated substrates were then cured at 150°C for 20 min. The resulting PDMS-AAP photo composites were transparent and could easily peel off form the substrates.

#### C. Surface characterization

Surface morphology of the composites was investigated with JEOL 6390 scanning electron microscope for structuring or clusters that would indicate phase segregation. A snippet of each composite was cut and peeled off for the imaging, which was done at (i)  $1 \text{ kV}/180 \times \text{magnification}$  and (ii)  $13 \text{ kV}/95 \times \text{magnification}$ .

#### D. UV-vis spectroscopy

Optical properties of the composites were determined via absorbance spectra recorded with Shimazu 3600 spectrophotometer in UV-vis range and compared to that of plain PDMS film of same thickness. A free space baseline was set in 270–800 nm wavelength range to eliminate stray interference and ensure that only absorbance of composites and PDMS films were recorded. A snippet of each sample was peeled off and mounted on sample holder for measurements. First, absorbance spectrum of the plain PDMS was acquired as a reference to be used to assess deviations in the composites because of the integrated photoswitch. Measurement on the composites was done in two stages: (i) before UV irradiation, when embedded molecules were in the *trans* state and (ii) after 5 min UV ( $\lambda = 365$  nm) irradiation when molecules were in *cis* state. We tagged these stages pristine and UV, respectively. The 5 min exposure time was informed by prior observation that our AAPs achieve photo-stationary state (maximum *trans-cis* conformational change) at this duration. The refractive indices of the plain PDMS and the composites were then determined from their absorbance spectra.

# 2.1 Fabrication of the PDMS-AAP Composite Thin Film via Spin-Coating Method

The AAP molecular switch in this project was synthesized using commercially available reagents. Preparation of the PDMD-AAP matrix was carried out using polydimethylsiloxane (PDMS) (elastomer and curer) of the Sylgard 184 silicone elastomer kit and AAP solution via spin-coating method. First, 0.10 g of the AAP molecular switch was dissolved in 10 mL of acetone to make 0.025 M solution at room temperature, as shown in Fig 1(b).

Next, the PDMS elastomer and curer are stirred in a 10:1 weight ratio. Then, 1.0 mL of the 0.025 M solution of the AAP was poured into 20 g of PDMS matrix and stirred for few minutes to make a homogeneous clear gel as shown in Fig 1(c). The uniform gel is spin-coated on the microscope slide at a high-speed of 2500 rpm for 2 min to make 75  $\mu$ m thin film. Then, the coated gel is baked at 150°C on a hotplate for 20 min. This procedure was repeated with different concentrations of the AAP photoswitch to fabricate different PDMS-AAP composite thin films to probe the effect of the concentration of the AAP photoswitch on the isomerization process and thickness of photochromic film.

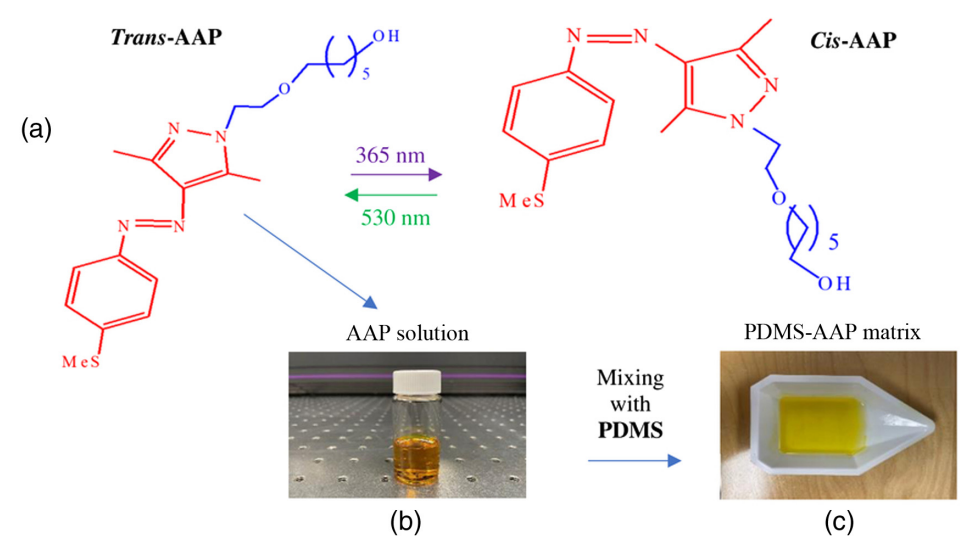


Fig. 1 (a) Chemical structure and photoswitching behavior of the AAP moiety; and (b)–(c) fabrication process of the PDMS-AAP matrix.

# 2.2 Fabrication of the PDMS-AAP Waveguide via the Photolithography Process

#### 2.2.1 Design of the primary mold

The grooves of the PDMS clad are designed and printed on the mylar mask. As shown in Fig 2(a), each square of the nine on the mold mask contains multiple rectangular-shaped channels with different dimensions and gaps in micrometer scale. The mask was designed with CAD software and the mylar mask was made by Artnet Pro, as shown in Fig 2(b).

#### 2.2.2 Making the PDMS replica mold

The mylar mask is used to fabricate the primary mold in contact lithography process. First, the negative resist (SU-8 3025) is spin-coated on a 3 in. wafer with 2500 rmp for 48 s to give a 20  $\mu$ m thick film. The coated wafer is then soft-baked for 10 min at 95°C. In the contact lithography step, the mylar mask is placed between a quartz and the photoresist-coated mold wafer to print the channels on the wafer. The wafer is exposed to UV light for 15 s and then baked at 95°C for 5 min. In post exposure step, the wafer is developed in propylene glycol monomethyl ether acetate (Sigma Aldrich 484431-4L) for 10 min and rinsed with isopropanol alcohol, as shown in Fig. 3. Finally, the wafer is baked for 5 min at 150°C after development.

In order to make the PDMS replica mold, 30 g Silgard is blended with 3 g curer and stirred with conditioning mixer and bubbles in the matrix are removed using a desiccator. Then, the PDMS is poured into the primary mold wafer and baked in an oven at 70°C for 1 h. The PDMS replica was peeled off from the mold wafer [Fig. 4(a)]. To fabricate the photoswitch

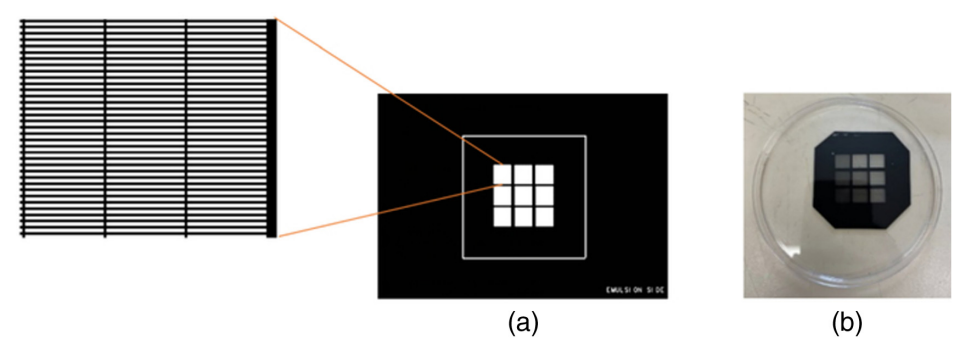


Fig. 2 Design of the mask in (a) CAD and (b) primary mylar mask.

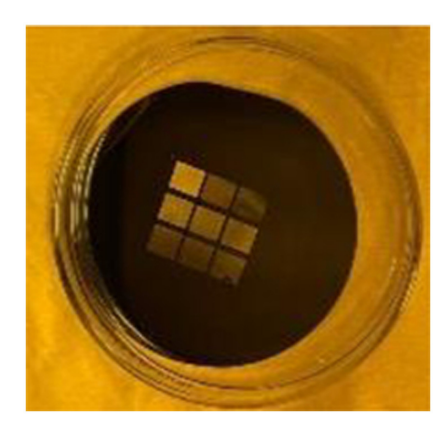


Fig. 3 Primary mold wafer coated with negative photoresist in lithography room.

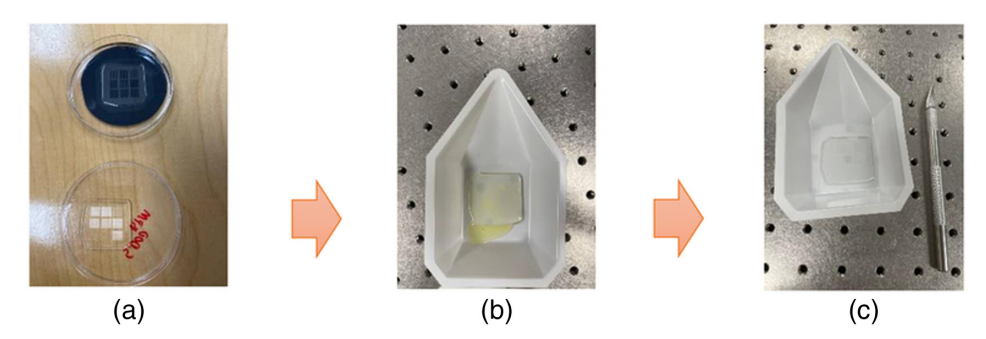


Fig. 4 (a) PDMS replica mold peeled off from primary wafer, (b) PDMS-AAP poured into the grooves of PDMS replica, and (c) extra PDMS-AAP matrix removed around the grooves with blade.

waveguide, the PDMS-AAP is poured into the groves of PDMS replica [Fig 4(b)]. The extra PDMS-AAP matrix around the grooves was removed by blade or pallet knife after a couple of hours, as shown in Fig 4(c).

# 2.2.3 Morphology of the PDMS-AAP composite film

The SEM images of the PDMS replica mold are displayed in Figs. 5(a) and 5(b). The SEM images show that the width of the canals is  $27.3~\mu m$ . Figure 5(c) shows image of the PDMS-AAP filled replica channels. Although the fabricated PDMS features have the size of micrometer, this initial photolithography study gives a clear idea for the next phase of the project, making the nanoscale hollows of the primary and replica molds with nanoimprint lithography method.

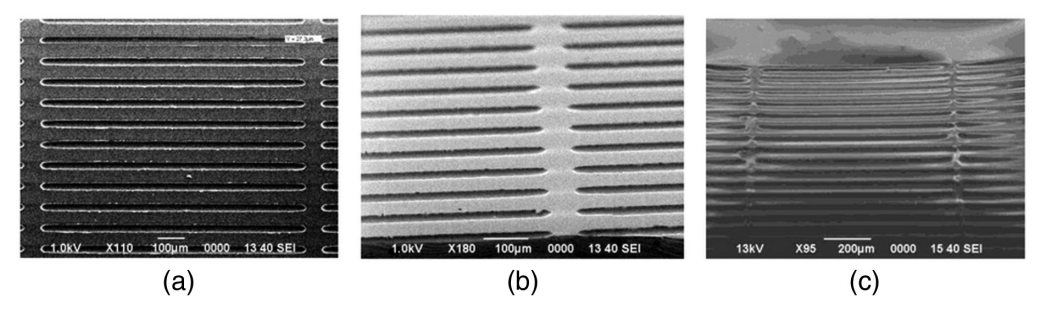


Fig. 5 (a), (b) SEM images of the PDMS replica mold, and (c) the replica channels filled with PDMS-AAP.

#### 3 Results and Discussion

#### 3.1 Simulation of the E-Field Profiles of the Waveguide

### 3.1.1 Wave confinement in PDMS-AAP waveguide with Maxwell equations

In our previous work, we designed the buried waveguide structure composed of 320 nm thick PDMS-AAP as the core surrounded by plain PDMS. The refractive index of the embedded PDMS-AAP is maximum at the operating wavelengths of 340 and 450 nm during the reversible isomerization process by the UV-visible regulating sources. <sup>10,11</sup> The 640 nm thick pliable PDMS clad/substrate is transparent to the UV-green regulator light, so the light reaches the immersed PDMS-AAP with the least attenuation. In this study, wave confinement was investigated with Maxwell's equations in the isomeric states of the composite core for different design properties. Based on the effective index method, <sup>10</sup> the waveguide structure was defined in terms of normalized parameters, shown in Eq. (1), for the wave  $E_y(x) = E_o(x, y)e^{i(\beta z - \omega t)}$  polarized in the y and propagating in z direction, where v is a v-number (normalized frequency), b represents the relative index, and  $\alpha$  is the asymmetry factor. <sup>10</sup>

$$v\sqrt{1-b} = (m-1)\pi + tg^{-1}\sqrt{b/(1-b)} + tg^{-1}\sqrt{(b+\alpha)/(1-b)} \quad \text{and} \quad \alpha = \frac{(n_{\text{clad}}^2 - n_{\text{sub}}^2)}{(n_{\text{core}}^2 - n_{\text{clad}}^2)}.$$
(1)

For a specific waveguide design, the normalized frequency at operating wavelength  $\lambda$  is related to the core thickness and indices, as shown in Eq. (2):<sup>23</sup>

$$v = \frac{2\pi d}{\lambda} \sqrt{(n_{\text{core}}^2 - n_{\text{clad}}^2)}.$$
 (2)

Figure 6 shows the b-v plot for the waveguide where the vertical red line marks the v-number in trans state. At the operating wavelength of 340 nm, three modes of the waveguide in the trans state are observed at the normalized frequency v=7.0. However, in the cis state, only one mode is detected in at normalized frequency v=2.4 for the same operating wavelength. The v-numbers are calculated in the same way for 450 nm, based on b values.  $^{10}$ 

# **3.1.2** Propagation modes extraction of PDMS-AAP waveguide using Ansys HFSS

In this work, the photoswitchable waveguide is simulated with finite element method, as shown in Fig. 7. The PDMS-AAP core has a dimension of 320 nm, surrounded by 160 nm plain PDMS for each side of the cube. The overall PDMS thickness and length is  $640 \times 640$  nm. The excitation ports were designed with floquet ports on top and bottom of the vacuum box in z-direction, while primary/secondary boundary conditions were considered for four sides of the vacuum rectangular cuboid. The number of modes can be adjusted in the floquet ports.

In our previous work, we studied the reversible refractive index modulation of a photoswitchable PDMS-AAP based composite films. As shown in Fig. 8, upon irradiation with

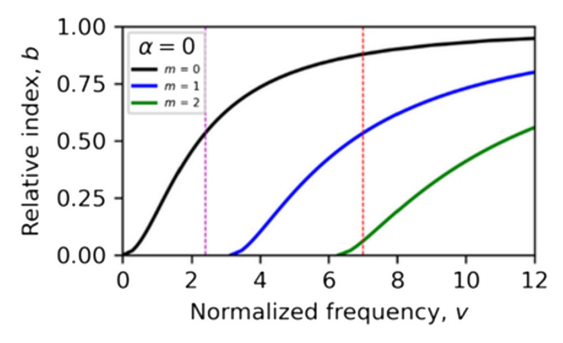


Fig. 6 Relative index/normalized frequency chart for 320 nm-thick PDMS-AAP core at operating wavelengths 340 and 450 nm.<sup>10</sup>

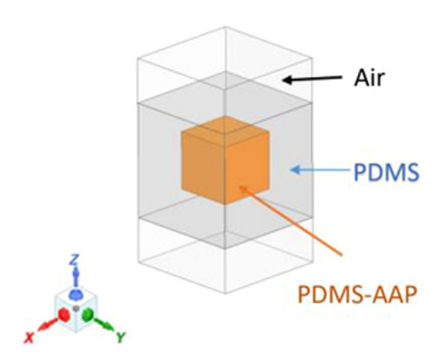


Fig. 7 Photoswitch waveguide structure designed with Ansys HFSS.

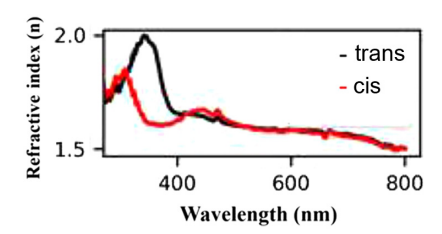


Fig. 8 Refractive indices of PDMS-AAP core measured for trans and cis. 11

light of specific wavelength, the AAP unit embedded in the PDMS-AAP matrix underwent reversible trans-to-cis isomerization, which was manifested by a drop in absorbance of the maximum absorption band at ~340 nm and by decrease in the refractive index. The measured refractive index of the embedded AAP core is used to compare the two numerical methods (Maxwell and finite element) for both the cis and trans states upon alternating illumination with UV ( $\lambda = 365$  nm) and green ( $\lambda = 525$  nm) light, respectively. Figure 8 shows the refractive index values of the PDMS-AAP composite from our previous study. At the operating wavelength of 340 nm, the refractive index reached to maximum 2.0 in the trans state. In the cis state, the core index at operating wavelength of 450 nm is 1.65. However, the refractive index of the organic core does not change significantly beyond 450 nm for trans and tis states. The PDMS index does not have notable variation at operating wavelengths 340 and 450 nm for both isomeric states.

In this study, the refractive index of the PDMS-AAP composite fabricated using a new photoswitch was measured based on the absorption spectra of the film using different molar concentrations of the AAP unit for both the *trans* and *cis* states (Fig. 9).<sup>11</sup> The refractive index (n) of the composite for normal incidence is derived from Fresnel equation, as shown in Eq. (3):<sup>24</sup>

$$R = \frac{(n-1)}{(n+1)},\tag{3}$$

where R is the reflectance of the incidence light. The mathematical expression of reflective index is displayed in Eq. (4), where  $\varepsilon_r$  is the real dielectric constant. In Eq. (5), extinction

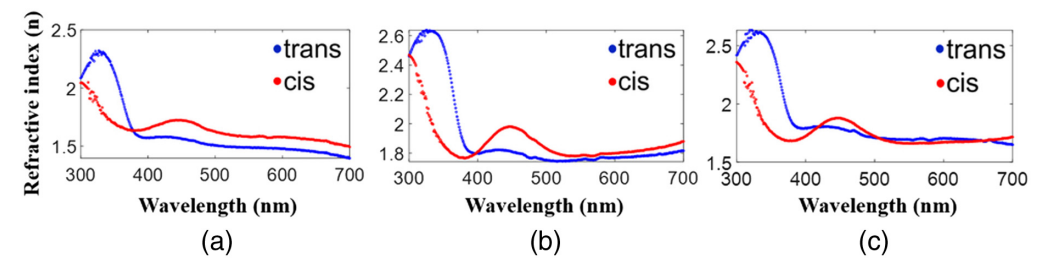


**Fig. 9** Refractive index of three different molarity concentrations (a) 0.01 M, (b) 0.02 M, and (c) 0.03 M of the PDMS-AAP composite thin film.

coefficient (k) is calculated based on the thickness (d) and absorption (A) of the thin film at certain wavelength  $(\lambda)$ :<sup>11</sup>

$$\varepsilon_r = n^2 - k^2,\tag{4}$$

$$k = 2.303 \frac{A\lambda}{4\pi d}. (5)$$

# 3.1.3 Sellmeier relation for the refractive index of PDMS-AAP composite

The refractive indices of the composite material exhibit a nonlinear response to wavelength in UV-visible light range. Considering the visible region, the response decreases monotonically such that Sellmeier equation can be used to describe the index variation for transparent medium. However, since conformation occurs in the UV region where significant photon energy absorption and  $\pi - \pi *$  transition register, one may consider a modified generalized Sellmeier equation to capture the contributions in the UV region. Such an approach has been explored in which the parameters of the Sellmeier equation were made complex entities. We adopt a different approach to maintain the real nature of the Sellmeier parameters and calculate the fitted data for the measured refractive indices of the composite. The general form of the Sellmeier equation is shown as  $^{26}$ 

$$n^2(\lambda) = A_o + \sum_{j=1}^m \frac{A_j \lambda^2}{\lambda^2 - B_j},\tag{6}$$

where  $A_o$  is a constant,  $A_j$  and  $B_j$  are Sellmeier coefficients, and  $\lambda$  is the wavelength. It is traditional to fit Eq. (6) with as many terms as possible to index data. However, a single term form of Sellmeier equation is shown as

$$n^{2}(\lambda) = A_{o} + \frac{A\lambda^{2}}{\lambda^{2} - B} = A_{o} + A \left[ \frac{1}{1 - B/\lambda^{2}} \right].$$
 (7)

The second term in Eq. (7) renders itself to the series form,  $A\sum_{m=1}x^m$ , in Eq. (8):

$$n^{2}(\lambda) = A_{o} + A + AB\left(\frac{1}{\lambda^{2}}\right) + AB^{2}\left(\frac{1}{\lambda^{2}}\right)^{2} + \dots = a_{o} + a_{1}x + a_{2}x^{2} + \dots$$
 (8)

Equation (8) is modified Sellmeier relation used in this work. The original Sellmeier parameters may be recovered by equating the first two coefficients of Eq. (8). Considering  $A + A_0$  as coefficient  $a_0$ , AB as coefficient  $a_1$ , and  $AB^2$  as coefficient  $a_2$ , Sellmeier coefficient  $A_0$ , A, and B are determined as

$$A_0 = a_0 - \frac{a_1^2}{a_2}, \quad A = \frac{a_1^2}{a_2} \quad \text{and} \quad B = \frac{a_2}{a_1}.$$
 (9)

The square root of the fitted refractive indices (n) at wavelength  $(\lambda)$  in Eq. (8) are determined by the modified Sellmeier coefficients  $(a_i)$  and original Sellmeier coefficients  $(A_0, A, A)$  and  $(A_0, A)$  based on the least square method, as depicted in Table 1. The fitted data of the eighth power of Eq. (8) show very good agreement with measured index of the 0.02M PDMS-AAP thin film in  $(A_0, A)$  and  $(A_0, A)$  thin film in  $(A_0, A)$  the fitted data of the eighth power of Eq.  $(A_0, A)$  and  $(A_0, A)$  thin film in  $(A_0, A)$  the fitted data of the eighth power of Eq.  $(A_0, A)$  the eighth po

In the *trans* state [Fig 9(a)], the refractive index maxima of the 0.01 M composite is 2.32 at 327 nm, whereas in the *cis* state the index of the film drops to 1.85. On the other hand, the maximum index for the *cis* state was 1.72 at 450 nm wavelength. Notably, as significant increase in the refractive index change was observed when the concentration increased to 0.020 and 0.03 M. Refractive indices of the 0.02 and 0.03 M solutions of the AAP in the PDMS-AAP composite were 2.65 in the *trans* state and 2.1 in the state at an operating wavelength of 326 nm [Figs. 9(b) and 9(c)]. These show that refractive index can be effectively tuned by changing the concentration of the azo dye embedded in the polymeric composite film. In addition, these results indicate a remarkable enhancement of the refractive index change compared with

Table 1	Modified Sellmeier coefficients	s and original parameters	for first-term Sellmeier Equation.
---------	---------------------------------	---------------------------	------------------------------------

Coefficients	Trans	Cis
$\overline{a_o}$	-115.68	-71.334
<i>a</i> <sub>1</sub>	204,557,472.8	129,094,056.7
$a_2$	-1.45194E + 14	-9.10058E + 13
$a_3$	5.55231E + 19	3.42086E + 19
$a_4$	-1.25332E + 25	-7.53867E + 24
$a_5$	1.71447E + 30	1.00513E + 30
$a_6$	-1.39268E + 35	-7.98414E + 34
a <sub>7</sub>	6.16899E + 39	3.48142E + 39
<i>a</i> <sub>8</sub>	-1.14643E + 44	-6.4216E + 43
$A_0$	172.51	111.7888
Α	-288.193	-183.123
В	-709793.35	-704957.25

our previous study.<sup>10</sup> We also presume that the different structure of the newly designed AAP may have played a role in enhancing the refractive index changes.

The propagation modes of the optical waveguides obtained based on the frequency versus imaginary part of the gamma are shown in Fig. 11. At frequencies higher than 656 THz, three modes of the PDMS-AAP based waveguide are observed in the *trans* state. Similar to the effective index method, we see only one mode in the *cis* state at frequencies lower than 470 THz. It should be mentioned that based on Fig. 8, the refractive index of the waveguide core is 1.63 at 450 nm in the *trans* state, which implies that we could see only single mode at lower frequencies. The relation between the imaginary part of the gamma in the finite element method and relative index b in the effective index method is explained in Eq. (10). The propagation modes of the photoswitch structure show excellent agreement for the two methods of Maxwell Equation in Fig. 6 and frequency dependent finite element method described in Fig. 11.<sup>10</sup>

$$E_y = E_0(x, y)e^{i\beta z} = E_0(x, y)e^{\gamma z}$$
 and  $\beta = n_{\rm eff} k_0$   
then  $\gamma = i\beta = i \ n_{\rm eff} k_0$  where  $b = \frac{n_{\rm eff}^2 - n_{\rm clad}^2}{(n_{\rm core}^2 - n_{\rm clad}^2)}$ . (10)

The transverse e-field profiles in the core are simulated on excitation ports of the structure in  $\hat{z}$  direction. Three fundamental modes (TE0, TE1, and TE2) of the waveguide in the *trans* state are observed on the PDMS-AAP core at frequency of 700 THz as shown in Fig. 12(a). The

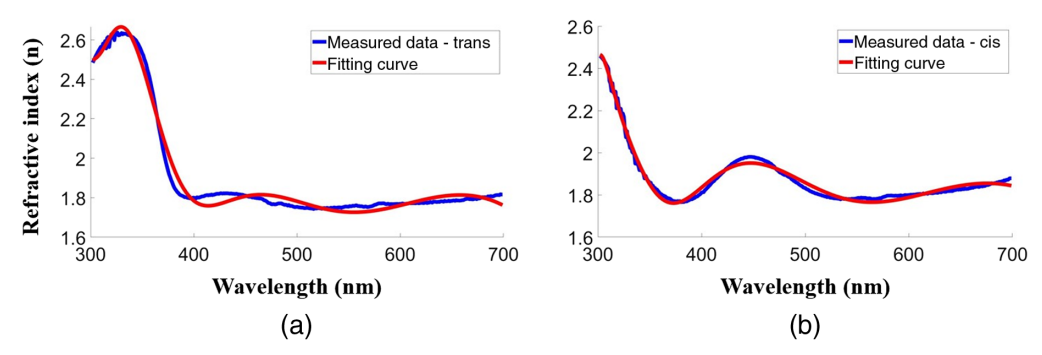


Fig. 10 Comparison of the fitted data and measured data by spectroscopy in (a) green and (b) UV light for the 0.02M composite film.

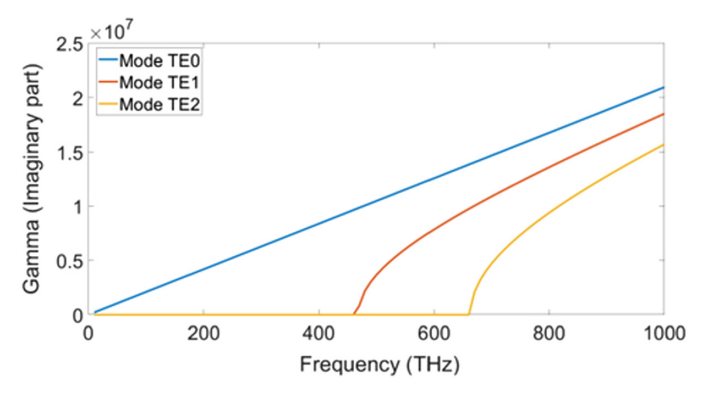


Fig. 11 HFSS simulation of wave propagations of optical waveguide in *cis* and *trans* isomeric states.

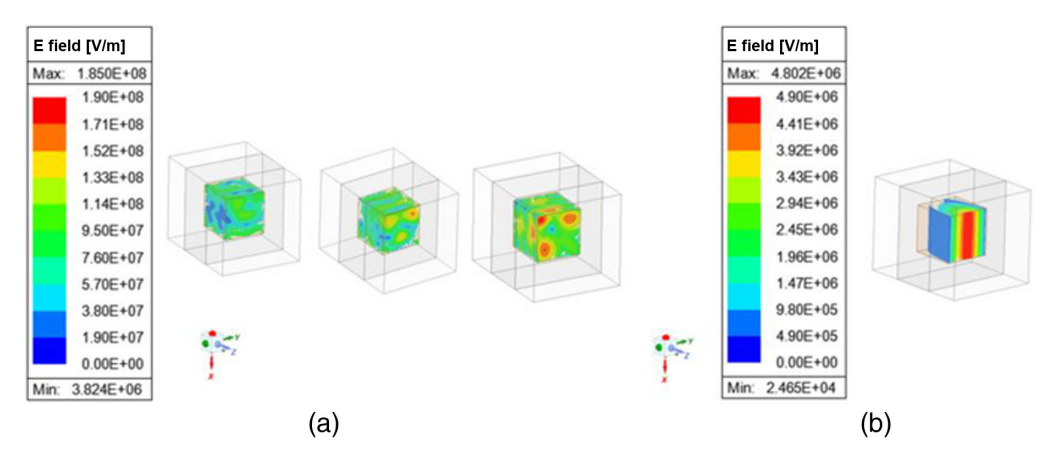
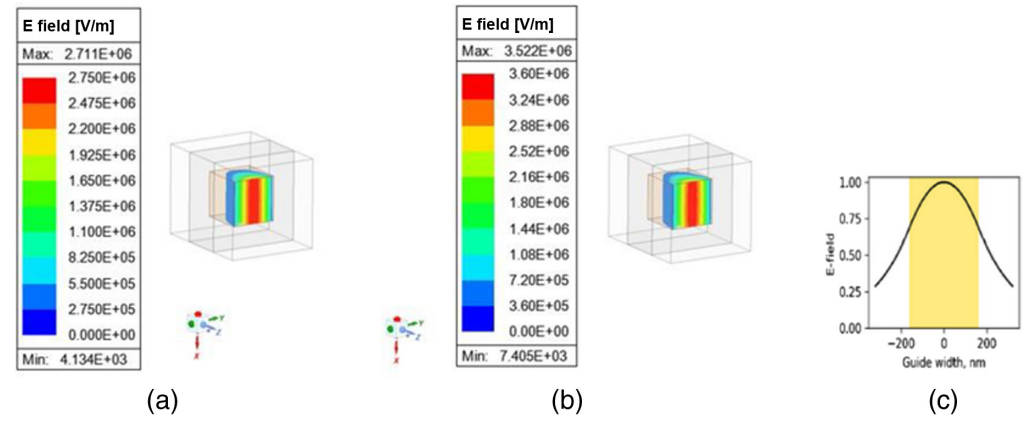


Fig. 12 Transverse electric field profiles of the PDMS-AAP buried waveguide at an operating wavelength of 340 nm in the (a) *trans* and (b) *cis* states analyzed by HFSS.

waveguide core in the *cis* isomeric state simulated at an operating wavelength of 340 nm shows single mode [Fig. 12(b)]. In the *cis* state, all higher modes are suppressed at lower frequency of 240 THz due to the resulting refractive index change by photoisomerization process. At an operating wavelength 340 nm, the refractive index of the core reaches to 2 and 1.65 for *trans* and *cis* states, respectively, as shown in Fig. 8.

Furthermore, the transverse electric field modes of the photoswitch core are analyzed in the visible region as described in Fig. 13. At an operating wavelength of 450 nm, the PDMS-AAP



**Fig. 13** Transverse electric field profiles in PDMS–AAP buried waveguide at wavelength 450 nm in (a) *trans* and (b) *cis* states by HFSS. (c) Electric field profile in the *cis* state generated via closed-form analysis of Maxwell Equations; shaded region is the PDMS-AAP core. <sup>10</sup>

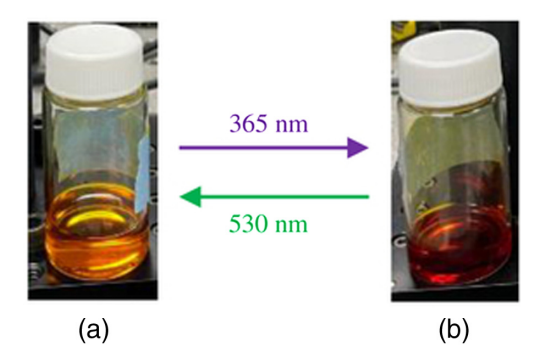


Fig. 14 Photochromic changes of AAP molecular switch dissolved in acetone upon irradiation of (a) UV ( $\lambda = 365$  nm and (b) green ( $\lambda = 530$  nm) lights.

buried core supports only one mode at frequencies lower than 470 THz. Interestingly, the number of modes can be increased in the *cis* state by changing the thickness of the photoswitch core. At wavelength 450 nm, the refractive index of the core is 1.63 in pristine and 1.67 in UV light, as described in Fig. 8. For comparison purpose, TE profiles of the PDMS-AAP composite are simulated at 160 and 200 THz in the *trans* and *cis*, respectively. The results show that there is good agreement with the finite element method [Figs. 13(a) and 13(b)], and the closed-form analysis of the waveguide in Figs 13(c). Thus, the independent finite-element simulation re-affirms waveguiding ability of the composite and validates the closed-form analysis described in our previous report.

### 3.1.4 Photochromic properties of the buried waveguide structure

The photochromic characteristic of the AAP molecular switch was examined in the UV-visible region. The color of the AAP-acetone solution changes to dark orange after irradiation with UV light for 5 min, as shown in Fig 14(b). The same solution changes its color back to bright yellow as pristine upon irradiation with 530 nm [Fig 14(a)], due to the reversible isomerization of AAP molecular switch.

### 4 Photoisomerization Spectral Characterization

#### 4.1 UV-vis Spectral Characterization of the PDMS-AAP Composite Film

The photoisomerization responses of the PDMS-AAP composite thin film in the solid-state was characterized by UV-vis spectroscopy. The changes in the UV-vis absorption spectra of the AAP unit embedded in the composite film as a function of time are shown in Fig. 15. As shown in Fig. 15, the UV-vis absorption spectra of the PDMS-AAP composite film display characteristic picks of the *trans-to-cis* isomerization of the embedded AAP unit upon irradiation with UV light at  $\lambda = 365$  nm and green light at  $\lambda = 525$  nm, respectively. The absorbance spectra of the composite film show intense band at 340 nm and weak bands at 440 to 450 nm in the visible

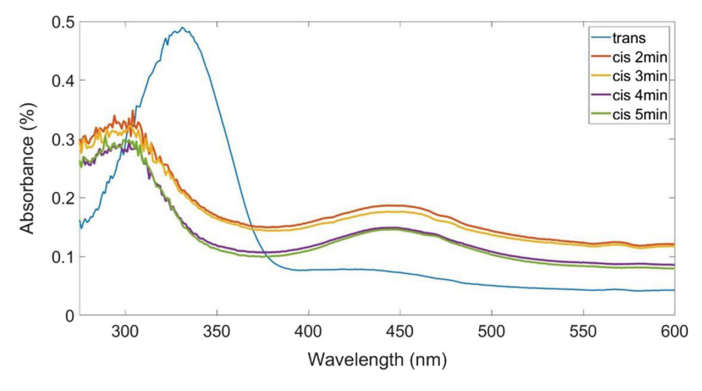


Fig. 15 Experimental UV-vis spectroscopy of PDMS-AAP.

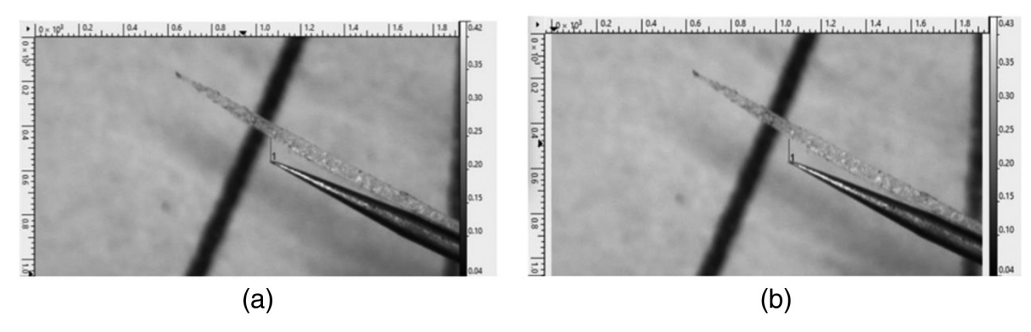


Fig. 16 Microscope images of the thin photochromic layer on the needle in (a) *trans* and (b) *cis* states.

Table 2 Measuring the film by alternative exposure of UV and green light at room temperature.

Irradiation	Distance	Remark
Green light (trans)	26.59 μm	Initial width
UV light (cis)	26.85 μm	Away from needle

region, which is characteristic features of the *trans*-isomer. Upon irradiation with UV light ( $\lambda=365$  nm) for 2 to 5 min, the *trans*-form of the AAP unit embedded in the polymer matrix was easily converted to the *cis*-isomer, resulting in new absorption bands at 290 and 450 nm. This was also clearly shown by significant decrease in the absorbance of the maxima at 340 nm and increase of the 450 nm band, which is indicative of the formation of the *cis*-isomer. This observation shows both the relatively fast *trans-to-cis* isomerization of the AAP molecular switches embedded in the polymer matrix and tunability of the optical properties of the composites. The new AAP molecules in this work can be addressed using higher energy UV light (e.g.,  $\lambda=254$  nm). However, the destructive nature of higher energy UV light is not preferred for the waveguide and other potential biological applications. As such, the main goal of this study is to shift the wavelength to visible or NIR range for the future works.

#### 4.2 Mechanical Characterization of the PDMS-AAP Thin Films

To study the photomechanical behavior, a thin slice of the PDMS-AAP composite film is placed on the needle as shown in Fig. 16. The photomechanical motion/actuation of the light-responsive solid-state thin film was then monitored with a microscope. The results show that the slice thin film bend ~200 nm away from the light source after radiation with UV light ( $\lambda = 365$  nm) for 5 min (Fig. 16). The distance of the 45 45  $\mu$ m thick layer from the needle is measured with Gwyddion software in Table 2.

#### 5 Conclusion

In this work, we have designed and theoretically simulated a light-responsive waveguide that exhibit efficient reversible *trans-to-cis* photoisomerization of an AAP unit embedded in a PDMS polymer matrix. The PDMS-AAP composite film was fabricated by mixing the photochromic AAP moiety into the flexible PDMS matrix via spin-coating. In addition, a solid-state waveguide was fabricated by soft lithography and replica modeling methods with the aim to construct nanometer scale channels. The propagation modes of the composite film were also simulated with finite element method, tuned by the refractive indices of the waveguide in isomeric states upon alternating irradiation with UV and green lights. The results were in good qualitative agreement with the closed-form refractive index analysis described in our previous work, thereby re-establishing the wave-guiding property of the composite. It has also been shown that the concentration of the AAP unit embedded in the composite film plays an important role, in which increasing concentration has been demonstrated to significantly enhance the refractive index changes.

The molecular force of the synthesized photoswitching thin film in this research has shown the mechanical bending stress and chromogenic response during isomeric states. These remarkable photo-induced refractive index changes suggest the potential applicability of the PDMS composite film doped with the novel AAP azo dyes for nanophotonic optomechanical platforms, including stress sensing systems. The development of mechanical stress-sensitive subwavelength materials enables changing the light–matter interactions due to their ability to show the mechanical activation in light responsive polymers.

#### Code, Data, and Materials Availability

Data are available from the authors upon request.

#### Acknowledgments

This paper was presented at SPIE Photonics West conference in San Francisco, California, on February 2, 2023.<sup>27</sup> National Science Foundation (NSF) supported this work through Grant NSF-DMR 1827820 for Partnership for Research and Education in Materials (PREM). We would like to show our gratitude to Breon Mccray, Anthony Gillespie, and Jihaad Barnett for assisting in constructing the UV/green lights and synthesizing the composite film.

#### References

- A. Shishido, "Rewritable holograms based on azobenzene-containing liquid-crystalline polymers," *Polym. J.* 42, 525–533 (2010).
- R. M. Parker et al., "Using the photoinduced reversible refractive-index change of an azobenzene co-polymer to reconfigure an optical Bragg grating," J. Mater. Chem. 20, 9118–9125 (2010).
- M. D. A. Babalhavaeji et al., "Red shifting azobenzene photoswitches for in vivo use," Acc. Chem. Res. 48, 2662–2670 (2015).
- D. Bleger and S. Hecht, "Visible-light-activated molecular switches," Angew. Chem., Int. Ed. 54, 11338– 11349 (2015).
- T. Xu et al., "Multiphotoinduced bending of azobenzene-modified graphene oxide/poly(vinyl alcohol) composite films for smart devices," ACS Appl. Nano Mater. 4, 10209–10217 (2021).
- Z. Mahimwalla et al., "Azobenzene photomechanics: prospects and potential applications," *Polym. Bull.* 69, 967–1006 (2012).
- 7. C. E. Weston et al., "Arylazopyrazoles: azoheteroarene photoswitches offering quantitative isomerization and long thermal half-lives," *Am. Chem. Soc.* **136**, 11878–11881 (2014).
- M. Schnurbus et al., "Smart air-water interfaces with arylazopyrazole surfactants and their role in photoresponsive aqueous foam," *Langmuir* 34, 6028–6035 (2018).
- 9. K. Ghebreyessus et al., "Solid-state photoswitching in arylazopyrazole-embedded polydimethylsiloxane composite thin films," *J. Solid State Chem.* **303**, 122519 (2021).
- I. Uba et al., "A study of wave confinement and optical force in polydimethlysiloxane-arylazopyrazole composite for photonic applications," *Polymers (Basel)* 14, 896 (2022).
- I. Uba et al., "Tunable optoelectronic properties of polydimethylsiloxane-arylazopyrazole flexible composite," in SoutheastCon IEEE (2021).
- 12. C.-W. Chu et al., "Light-responsive arylazopyrazole gelators: from organic to aqueous media and from supramolecular to dynamic covalent chemistry," *Chem. Eur. J.* **25**, 6131–6140 (2019).
- 13. Y. Yu and T. Ikeda, "Alignment modulation of azobenzene-containing liquid crystal systems by photochemical reactions," *J. Photochem. Photobiol.*, *C* 5, 247–265 (2004).
- 14. M. Schnurbus et al., "Photo-switchable surfactants for responsive air—water interfaces: azo versus arylazo-pyrazole amphiphiles," *J. Phys. Chem. B* **124**, 6913–6923 (2020).
- W. C. Chuang et al., "Fabrication of optical filters based on polymer asymmetric Bragg couplers," *Opt. Express* 17(20), 18003–18013 (2009).
- D. Garcia-Rodriguez et al., "Bimodal grating coupler design on SOI technology for mode division multiplexing at 1550 nm," Opt. Express 26(15), 19445–19455 (2018).
- 17. P. Dong and H. W. Yang, "Guided modes in slab waveguides with both double-negative and single-negative materials," *Opt. Appl.* **40**(4), 873–882 (2010.)
- 18. K. Kawano and T. Kitoh, Introduction to Optical Waveguide Analysis, John Wiley & Sons, Inc. (2001).
- G. Mirbagheri, D. T. Crouse, and C.-K. Tan, "Recent advance in phase transition of vanadium oxide based solar reflectors and the fabrication progress," *Proc. SPIE* 11995, 1199500 (2022).

- D. T. Nguyen et al., "An arylazopyrazole-based n-heterocyclic carbene as a photoswitch on gold surfaces: light-switchable wettability, work function, and conductance," Angew. Chem. Int. 59, 13651–13656 (2020).
- G. Mirbagheri and D. T. Crouse, "Design, fabrication, and spectral characterization of temperature dependent liquid crystal-based metamaterial to tune dielectric metasurface resonances," *Proc. SPIE* 12000, 120000K (2022).
- R. W. Barber and M. J. Robb, "A modular approach to mechanically gated photoswitching with color-tunable molecular force probes," *Chem Sci* 12, 11703–11709 (2021).
- I. Mathews et al., "Towards AlN optical cladding layers for thermal management in hybrid lasers," *Proc. SPIE* 9520, 95200J (2015).
- 24. C. A. Mack, Field Guide to Optical Lithography, SPIE Press, Bellingham, Washington (2006).
- S. Moghaddam and S. K. O'Leary, "A Sellmeier extended empirical model for the spectral dependence of the refractive index applied to the case of thin–film silicon and some of its more common alloys," J. Mater. Sci. -Mater. Electron. 31, 212–225 (2020).
- S. Heshmatia, H. Taleb, and A. Rahmani, "Complex Sellmeier equation for the refractive index of semiconductors in the opaque region," Optik—Int. J. Light and Electron Opt. 172, 851–854 (2018).
- G. Mirbagheri et al., "Numerical analysis of the propagation modes of photo-switching PDMS-arylazopyrazole optical waveguide and thin-film spectroscopic characterization," *Proc. SPIE* 12424, 124241L (2023).

**Golsa Mirbagheri** is a research assistant professor at Hampton University. She received her PhD in Electrical and Computer Engineering from Clarkson University in 2020 and conducted post-doctoral research at Duke University in 2021. Her current research focuses on optics and opto-electronic materials, device design, metamaterial and micro/nanofabrication.

**Ikemefuna Uba** holds doctorate degrees in Condensed Matter Physics and Electrical Engineering from Nnamdi Azikiwe University and Howard University, respectively. His research activity is spread across semiconductors for electronic applications, spintronics systems and reliability of power electronics systems. His current research interest is in photo-responsive conducting polymers for flexible electronics, photoresponsive ferromagnets and magnetic semiconductors for spintronics and energy storage.

**Kesete Ghebreyessus** is an associate professor in the Department of Chemistry and Biochemistry. He received his PhD in chemistry from the University of Nevada-Reno in 2003. Prior to joining Hampton University in 2005, he did a postdoctoral research work at Iowa State University in the area of Alternative Energy Resources. His research interests and publication are in the areas of development of optically controlled molecular switches, materials chemistry, nanomaterials, and bioinorganic chemistry.

**Uwe Hömmerich** received his PhD in physics from the University of Hamburg (Germany) in 1994. Following a postdoctoral year at the University of Wisconsin-Madison, he joined the Department of Physics at Hampton University in 1995. His research interest includes fluorescence materials development, laser spectroscopy, rare earth doped solids, solid-state laser materials, crystal growth, laser-induced breakdown spectroscopy for chemical sensing. He has authored/co-authored more that 100 research papers in peer-reviewed journals.

**Seth Fraden** is a professor of physics at Brandeis University. He received his PhD in physics from Brandeis University. His research is focused on four topics; non-linear chemical dynamics, active matter, microfluidics technology, and colloidal self-assembly.

**Michael Stehnach** is currently a postdoctoral associate in the Department of Physics at Brandeis University. He earned his PhD in mechanical engineering from Tufts University in 2022, where he studied cell motility in inhomogeneous fluid environments. His current research involves implementing various microfabrication techniques to develop new microfluidic devices for studying active matter systems.

**Demetris Geddis** is the assistant dean of the School of Engineering, Architecture, & Aviation and chair of the Department of Electrical and Computer Engineering at Hampton University. He earned his Bachelor of Science in electrical engineering from Hampton University and Master of Science and PhD in electrical and computer engineering from the Georgia Institute of Technology. Current research interests and publications are in the areas of photonic integrated circuits, heterogeneous thin-film integration, and biophotonics.